Assessing the impact of very large volcanic eruptions on the risk of extreme climate events

ENVIRONMENTAL RESEARCH
CLIMATE

Assessing the impact of very large volcanic eruptions on the risk of extreme climate events

To cite this article before publication: Nicolas Freychet *et al* 2023 *Environ. Res.: Climate* in press https://doi.org/10.1088/2752-5295/acee9f

Assessing the impact of very large volcanic eruptions on the risk of extreme climate events

Nicolas Freychet[1], Andrew P. Schurer[1], Andrew P. Ballinger[1], Laura Suarez-Gutierrez[2,3,4], and Claudia Timmreck[2]

[1]School of Geosciences, University of Edinburgh, Edinburgh, UK

[2]Max Planck Institute for Meteorology, Hamburg, Germany

[3]Institute for Atmospheric and Climate Science, ETH Zurich, Zurich, Switzerland

[4]Institut Pierre-Simon Laplace, CNRS, Paris, France

July 21, 2023

Corresponding author: a.schurer@ed.ac.uk

Abstract

Very large volcanic eruptions have substantial impacts on the climate, causing global cooling and major changes to the hydrological cycle. While most studies have focused on changes to mean climate, here we use a large ensemble to assess the impact on extreme climate for three years following tropical and extratropical eruptions of different sulfur emission strength. We focus on the impact of an extremely large eruption, injecting 40 Tg sulfur into the stratosphere, which could be expected to occur approximately twice a millennium. Our findings show that the eruption would have a profound effect on large areas of the globe, resulting in extremely rare drought events that under normal circumstances would occur once every century becoming very likely. Several regions such as West Africa, South and East Asia and the Maritime continent are particularly affected with the expected climate shifting well outside the usual range, by up to 5 standard deviations. These results have important consequences as they indicate that a severe drought in multiple breadbasket regions should be expected following a large eruption . The risk of heavy rainfall tends to decrease over the same regions but by a reduced amount, heatwaves

become extremely rare however the chance of extreme Winter cold surges do not increase by a corresponding amount, since widespread parts of the Northern Hemisphere display a winter warming. Our results show that the location of the eruption is crucial for the change in extremes, with overall changes larger for a Northern Hemisphere eruption than a tropical and Southern Hemisphere eruption, although there is a regional dependency. Simulations of different eruptions with similar forcing distributions but with different sizes are consistent with a linear relationship, however for smaller eruptions the internal variability tends to become dominant and the effect on extreme climate less detectable.

1 Introduction

Explosive volcanic eruptions can inject large amount of various gases and particulates into the stratosphere, including sulfur containing gases such as sulfur dioxide, which can be converted into aerosol particles. These can have a major effect on the climate [e.g. Robock, 2000, Timmreck et al., 2012, Kremser et al., 2016] leading to a reduction of global mean surface temperature and the surface energy budget due to the reduced incoming solar radiation and a warming of the stratospheric aerosol layer due to the absorption of outgoing longwave radiation leading to global cooling [Robock and Mao, 1995, Timmreck et al., 2012]. Stratospheric aerosol concentration decreases with time, involving different chemical or physical processes, and the climate usually converges toward its baseline trajectory after a few years, although large eruptions can influence certain aspects of the climate for decades [Brönnimann et al., 2019]. This implies that, during a certain period of time, seasonal and interannual forecasts are potentially strongly impacted by a volcanic eruption.

Previous studies have detected changes in the hydrological cycle, including a global precipitation reduction following an eruption [Trenberth and Dai, 2007, Iles and Hegerl, 2014] although the pattern of change is non-homogeneous with many places expected to get dryer and some wetter [Iles and Hegerl, 2015, Zuo et al., 2019b]. In particular volcanic eruptions have been shown to have an important effect on tropical precipitation leading to a decrease in the summer monsoon region, due primarily to a weakening of the regional tropical overturning and a moisture reduction from volcanic cooling, a finding that is broadly supported by observations and modelling studies [e.g. Joseph and Zeng, 2011, Man et al., 2014, Paik and Min, 2017, Fadnavis et al., 2021, D'Agostino and Timmreck, 2022]. Further work highlighted that this tropical precipitation response is dependent on the climate model used [Paik et al., 2020] and the eruption latitude [e.g. Zuo et al., 2019a, Zhuo et al., 2021, Jacobson

et al., 2020].

Although the mean climate response to a volcanic eruption is already well established, less is understood about the response of climate extremes. This is due to the combined rarity of volcanic events and extreme climate events, making significant statistical analyses difficult to conduct, especially from observations. Moreover, very large volcanic eruptions such as the Samalas eruption in 1257, with 59.4 Tg sulfur emission in the stratosphere or the 1815 Tambora eruption with a stratospheric sulfur emission of 28.1 Tg (S) [Toohey and Sigl, 2017], have never been recorded directly during the satellite observation period (after 1980s). Yet the return period of a +40 Tg (S) eruption is estimated to be 500 years based on the data from Sigl et al. [2022], frequent enough to be plausible over the next century. The largest eruption, during the satellite era has been the Mount Pinatubo (15th June 1991), with 5-10 Tg of sulfur injected in the stratosphere [Quaglia et al., 2023]. Thus there is a lack of understanding on how a massive eruption such as the Tambora eruption could impact the occurrence of extreme weather events, and what it would mean for society. This is particularly important because eruptions have the potential to cause large climate effects simultaneously across multiple continents with potentially consecutive or sustained extreme climate events, and are therefore likely to lead to impacts larger than simply the sum of the individual events due to compounding and cascading impacts [Raymond et al., 2020, 2022]. It is thus crucial to assess what would be the consequences of such a volcanic event.

Two studies have investigated how some climate extremes respond to large tropical volcanic eruptions: Paik and Min [2018] used the Coupled Model Intercomparison Project Phase 5 (CMIP5, Taylor et al. [2012]) ensemble to investigate responses to eruptions over the historical period (1850-present day), while Wang et al. [2021] used two climate models run over the last millennium using CMIP5 volcanic forcing to investigate the response to eruptions since 850. Both studies found that temperature indices (annual minimum and maximum temperatures) closely follow the mean temperature response. Precipitation indices (5-day annual maximum precipitation and the Simple Precipitation Intensity Index (SDII)) were also found to be consistent with the mean response in precipitation, although the signal was less robust across models. These studies provide an important first step toward the evaluation of the relationship between volcanic events and climate extremes. However, the events as they were defined could be considered moderate extremes. Indeed, they mostly correspond to annual return period events, which are still frequent enough to be close to the mean climate response (e.g. Fig.3 and 7 from Paik and Min [2018]). High impact extremes, for which the society is less prepared,

happen with much lower frequencies such as once in a century. A common definition is, for example, to use these centennial return period events as low-probability high-impact events. This obviously requires extensive datasets to conduct robust statistical analysis, which was not possible in the previous studies. They both also focused on tropical eruptions combining the results from multiple often moderate volcanic eruptions of different emission strength.

Thus, there is an important need to address the question how do very large volcanic eruptions change the likelihood of high-impact low probability extreme events? This paper aims to answer this main question by taking advantage of large ensemble simulations, described in the Methodology section, while also investigating where in the world these risks are significantly changed and whether the response is sensitive to the location of the volcano and to the emission strength. The use of large ensemble simulations provides many occurrences of a given climate, enabling the efficient quantification of the internal variability [Maher et al., 2019, Deser et al., 2020, Milinski et al., 2020]. They also allow an estimate of the occurrence of high impact-low probability extremes [Fischer et al., 2021, Suarez-Gutierrez et al., 2020]. By comparing several large ensemble simulations with different climate conditions - here with or without volcanic eruptions - it becomes possible to efficiently quantify how the likelihood of extreme cases is changing, and how it compares with the internal variability. The setting of the simulations used in this study is presented in Section 2 along with the climate extreme indices analysed. Section 3 presents the results, and Section 5 provides discussion and concluding remarks.

2 Methodology

2.1 Model: MPI-EVA simulations

For this study, outputs from large ensemble simulation with the low resolution version of the Max Planck Institute Earth System Model (MPI-ESM1.1-LR) are used. The model couples the atmospheric general circulation model ECHAM6.3 (with a T63 horizontal grid, about 1.88°, and 47 vertical levels Stevens et al. [2013]) with the ocean-sea ice model MPIOM (with a GR15 horizontal grid, about 1.5°, and 64 vertical levels [Jungclaus et al., 2013]. It also includes the JSBACH3.0 land model [Reick et al., 2013] and the HAMOCC5.2 ocean biogeochemistry model.[Jungclaus et al., 2013]. Multi-model large ensemble evaluation studies show that the Max Planck Institute Grand-Ensemble (MPI-GE), which has 100 ensemble members for the historical period 1850-2005, run using the MPI-ESM1.1-LR model

Maher et al. [2019] offers one of the most adequate representations of the historical internal variability and forced changes in observed temperatures [Suarez-Gutierrez et al., 2021] and precipitation [Wood et al., 2021]. The model has also been used successfully to analyse the occurrence of high-impact, low-probability extremes [Suarez-Gutierrez et al., 2020].

Within the MPI-GE framework, the Easy Volcanic Aerosol ensemble [EVA-ENS; Azoulay et al., 2021] was specifically designed to disentangle the impact of a volcanic eruption from the climate internal variability. It uses the EVA volcanic forcing generator from Toohey et al. [2014] to generate idealized zonally and monthly mean volcanic aerosol optical properties (extinction, asymmetry factor, single scattering albedo) for a given stratospheric sulfur injection and eruption location. These optical parameters will be prescribed in the model's radiation scheme. Although many eruption magnitudes have been considered in EVA-ENS, here the focus is on a very large eruption, equivalent to 40 Tg of stratospheric sulfur injection. All eruptions are set to occur in June 1991 corresponding to the 1991 Pinatubo eruption. In addition to a tropical eruption, idealized eruptions (40 Tg) in the Northern and Southern Hemisphere extratropics are also considered; here these experiments are respectively referred to as EVA40, EVA40$_{NH}$ and EVA40$_{SH}$. All EVA cases consist of 100 ensemble members, each being initialised in January 1991 from one of the 100 members of the MPI-GE historical simulations and run for 3 years, leaving 2.5 post-eruption years to be analysed. In addition, an ensemble without volcanic eruption (hereafter EVA0) is used as a reference, and to evaluate the internal variability.

The EVA-ENS runs have been evaluated in Azoulay et al. [2021], Kroll et al. [2021], and D'Agostino and Timmreck [2022], with the latter focusing on the monsoon regional response. Here we focus on the response of several extreme climate indices while linking our results to the mean circulation change identified in previous studies.

2.2 Climate extreme events

This study focuses mostly on precipitation extremes as their sensitivity to volcanic eruptions is still poorly evaluated, but some results for temperature extremes are also presented. The different indices representing hydrological and temperature events in this study are shown in Table 1 and are: The maximum accumulated 5-day precipitation (Rx5d) which is used for assessing flood risk [Brönnimann et al., 2022]. The total accumulated precipitation (TP) and the total number of dry days (<1 mm/day, TDD) are used to assess stress on water resources and risk of drought. The minimum 3-day mean temperature (Tn3d) and the maximum 3-day mean temperature (Tx3d) (calculated as the average of

3 days of daily mean temperature) are used for cold surges and heat waves respectively. Each index is first computed for each month and grid point, and then aggregated over time and space to present seasonal or regional results, where indices over multiple days are calculated using a running-mean. All indices are calculated for both annual and seasonal periods and are computed individually for each member. Thus, for a given EVA case and for a given season or year, this corresponds to 100 samples of each index (100 members) which represent the internal variability of these events. Centennial events correspond to the highest (or lowest) 1% members, which in turn corresponds with the 99th percentile events with a 1-in-100 years return periods. However, to reduce the sensitivity to the sampling size, a generalised extreme value distribution (GEV) is fitted to the ensemble from which the 1% probability threshold is deduced. A GEV distribution has been chosen since it has been shown to be suitable to estimate changes in the probability of rare extreme events [Zwiers and Kharin, 1998], and is commonly used in extreme event attribution [e.g. Otto et al., 2018].

Note that TDD is a discrete (number of days) and bound (between 0 and 30 for a monthly result) variable. Fitting a distribution on such a variable, or even defining centennial events based on percentiles, may lead to unrealistic results, especially in very dry or wet regions (where TDD can be 30 or 0 respectively in each member). Thus, TDD will not be used for investigating centennial events.

2.3 Risk ratio of centennial events

To quantify the changes in risk between the reference case and EVA cases a risk ratio (RR) is used. This is a commonly used metric to express the change in probabilities of extreme events under climate change (NAS 2016). Here it is defined as the ratio of the probability of an event occurring in a world with the volcanic eruption to its probability in a world without the eruption, so it is a measure of how much more likely a particular event is due to the volcanic eruption. The following steps summarize RR computation for a given index, with EVA40x denoting any of the EVA40 cases, and two examples are shown for this procedure in the supplement (Supplementary Fig. S1 and S2):

1. Index is computed in EVA0 and EVA40x for the boreal winter and summer season the year following the eruption.

2. A GEV distribution is fitted separately to each ensemble.

3. Centennial event threshold is defined based on the EVA0-fitted GEV, and the probability to reach this threshold in EVA0 is P0.

4. Probability to reach this same threshold in EVA40x (P40) is computed based on the EVA40x fitted GEV.

5. The RR is computed as P40/P0.

Note that P0 corresponds here to 0.01 by definition (1% for a centennial event). A RR of 1 means there is no change in the extreme event's risk, while a RR higher (lower) than 1 indicates an increased (decreased) risk.

RR can be sensitive to the sampling. To evaluate the robustness of the results, a bootstrapping method is used. This consists of resampling (randomly) EVA0 and EVA40x before recomputing steps 2-5. The process is repeated 1000 times, and the 95% confidence interval is extracted from these 1000 RR estimations. The RR is significant if the confidence interval does not include 1, i.e. the RR is different from 1 with 95% confidence.

3 Results

3.1 Changes in the risk of seasonal extreme events

A focus is first made on the risk of centennial droughts (Fig.1), corresponding to the lower tail of the EVA0 TP distribution. Results focus on the boreal winter and summer seasons (DJF and JJA respectively) following the eruption.

For EVA40, it is clear that the immediate impact of a very large eruption is to significantly increase the risk of centennial droughts over a large part of land areas, in both seasons. The European continent's response is stronger during the first winter. A drying of the winter season, potentially translating to weaker snow cover, could have a strong impact on water resources for the following year. In monsoonal regions such as West Africa, South and East Asia or South America, the risk ratio shows a stronger signal during their respective summertime. This indicates a higher chance of monsoon failure, where precipitation would reach a centennial minimum. This could severely impact populations relying on monsoon precipitation. These results are in agreement with the general weakening of the monsoon following a volcanic eruption in these simulations previously found by [D'Agostino and Timmreck, 2022] and by other studies [e.g. Trenberth and Dai, 2007, Joseph and Zeng, 2011, Iles and Hegerl, 2014, 2015].

Regionally the risk of drought can be multiplied by more than 50, meaning that historical cen-

tennial events would become a 1 in 2 years events. In other words, over some regions a centennial drought would have a 50% chance of occurring following a very large eruption. This would have grave consequences for agriculture, farming and water resources at global scales, with the possibility of simultaneous crop failure in multiple breadbaskets [Gaupp et al., 2019]. The robustness of this signal, at least as analysed in this specific model experiment, suggests that immediate warnings and mitigation strategies should be implemented if such an eruption were to happen. The only regions showing a significant reduced risk in drought is Central North America and South Europe during summer.

Results for EVA40$_{NH}$ show broadly similar results but with a stronger signal. Thus the consequences of such an eruption could be even more severe. On the other hand, EVA40$_{SH}$ indicates almost no change over North Hemisphere land, and even a reduced risk over South Asia and the Sahel during summer, indicating an enhanced monsoon signal for this region, consistent with studies which have found similar patterns [Zuo et al., 2019a, Haywood et al., 2013, Liu et al., 2016], attributing the differences in monsoon behaviour to shifts in the intertropical convergence zone caused by asymmetric volcanic aerosol concentrations. West-Central Africa and the Maritime Continent, however, still show a significant increased risk of drought (although the signal is slightly shifted to the South for the former). These regions are thus highly vulnerable to very large eruptions no matter where the eruption takes place.

Changes in the risk of heavy rainfall are displayed in Fig.2. As Rx5d is on the other side of the precipitation distribution, one should expect to get an opposite signal to TP, if the distribution is shifted. Overall, the risk ratios for Rx5d are noisy and poorly significant, meaning that even a very large eruption does not systematically modify the occurrence of the most heavy precipitation for this signal to emerge clearly beyond the effect of internal variability. The most robust results are found in EVA40 and EVA40$_{NH}$ over South America and South Africa during DJF, and over West Africa during JJA, all showing a significant decrease in risk. EVA40$_{SH}$ does not show similar significant impact. Note that a strong positive risk ratio is also visible for West Africa during DJF (for EVA40 and EVA40$_{SH}$) and South-West America during JJA (for EVA40$_{NH}$). But precipitation over these regions is very weak during these respective periods as it corresponds to their dry seasons, and extreme RX5d events in these regions thus correspond to only small amount of precipitation.

Results for the temperature indices are displayed in Supplementary Figures S3 and S4. Although indices are displayed globally for both JJA and DJF seasons, the following discussion focuses on winter

and summer for cold surges and heat waves respectively.

Both temperature index risk ratios show a strong dependency to the volcano location. The risk of cold surges is significantly increased during the austral winter (JJA) for the Southern Hemisphere in EVA40 and EVA40$_{SH}$, but only in a small number of regions for EVA40$_{NH}$. On the other hand, during the boreal winter the risk of cold surges is reduced in the Northern Hemisphere for all EVA cases, with a stronger impact in EVA40$_{SH}$ and EVA40$_{NH}$. This is related to the Northern Hemisphere winter warming following an eruption, identified in previous studies [e.g. Robock, 2000, Bittner et al., 2016, Azoulay et al., 2021]. It is clear here that this warming is much stronger in a case of extra-tropical eruption than for a tropical one.

The risk ratio of heat waves is, not surprisingly, strongly reduced over a large part of the globe due to the overall global cooling caused by the stratospheric aerosols, especially for Northern Hemisphere summer heat waves (JJA) in EVA40 and EVA40$_{NH}$ (but not in EVA40$_{SH}$). The risk of South Hemisphere summer heat waves (DJF) is also reduced in EVA40, and in EVA40$_{SH}$ but not significantly. Thus the change in summer heat wave risks strongly depend on the volcano location. It is also noticeable that a significant increase in heat wave risk is shown for West India and South Asia during JJA in EVA40$_{NH}$. This can be related to the stronger shift in the monsoon following this volcanic eruption [D'Agostino and Timmreck, 2022], which would amplify the societal impact of drought identified previously.

3.2 How regional climate changes relative to natural variability

The risk ratios previously analysed are useful for quantifying the risk of reaching a certain extreme limit. Another way to look at the impact of a volcanic eruption on extremes is to evaluate whether the climate shifts outside of its natural variability, represented here by EVA0 ensemble variability. It is important as it shows how regional climates can shift to a totally different state and, unlike risk ratios, it does not focus on a specific threshold. We focus the analysis on several key regions: Europe, West Africa, the middle East, India, East Asia, and the maritime continent. Supplementary figure S5 shows the boundaries of the regions analysed as defined in the IPCC AR6 report [Iturbide et al., 2020]. Fig. 3 displays the results for each climate extreme index over these regions.

For precipitation indices the Maritime Continent and West Africa regions show the strongest shifts outside internal variability and here the change is toward more drought events (less accumulated precipitation; Tp) accompanied by less heavy rainfall (Rx5d), with extremely rare events (up to 5

standard deviations from the mean) becoming possible. A similar but weaker relationship also holds for India and East Asia. Overall the impact is weaker in EVA40$_{SH}$ except over the Maritime Continent. The Middle East is the only region where accumulated precipitation (Tp) increases (and therefore the chance of drought decreases), mostly for EVA40$_{NH}$.

For temperature extremes, it is clear that a massive shift occurs in Tx3d over five of the regions, namely India, East Asia, West Africa the Middle East and to a lesser extent Europe. In many parts of these regions for EVA40 and EVA40$_{NH}$ the shift is about 5 standard deviations of EVA0, well beyond what is often considered as the confidence interval of the internal variability (2 standard deviations). This means that following a very large Northern Hemisphere or tropical eruption, heat waves will be greatly suppressed in these regions. An important point is that this massive shift in heatwaves is not related to the same shift in cold events. Indeed, Tn3d does not show signals of similar magnitude as Tx3d in any of the above regions. Thus the systematic decreased risk in heat waves is not accompanied by a commensurate increase in the risk of cold events. Lastly, results for EVA40 and EVA40$_{NH}$ are very similar, but EVA40$_{SH}$ shows overall weaker signals except over India for Tn3d. The location of the eruption is thus an important factor to forecast the risk of systematic shift in regional climates.

The above results show that, depending on the volcano location, there are systematic shifts in extreme events over some regions, with several regions, such as West Africa experiencing significant changes in both temperature and precipitation events with shifts far beyond the internal variability. Thus society should be prepared to endure unprecedented weather events simultaneously across multiple regions.

3.3 Persistence of drought risk

In the previous sections, it was shown that very large eruptions can enhance the risk of drought across many regions. This section goes further by investigating the persistence of this signal over four particularly vulnerable regions: West Africa, Central Africa, the Maritime Continent, and India (Fig.4).

A strong reduction in monsoon precipitation occurs over West Africa immediately following the eruption in EVA40$_{NH}$ and persists for at least the following two years (a weak recovery seems to start in the second year). Precipitation is reduced by 50% each season and coincides with a doubling in the number of dry days. This monsoon failure is also apparent in EVA40, but with weaker magnitude and mostly during the year following the eruption. The number of dry days does not change significantly,

meaning that the reduction in precipitation is mostly due to reduced intensity. This slower response and a faster recovery in EVA40 compared to EVA40$_{NH}$ shows that the persistence of the drought risk in West Africa is highly dependent on the eruption location.

Over Central Africa a similarly fast and persistent decrease in the peak intensity of the rain season (centered around August) occurs in both EVA40 and EVA40$_{NH}$, although the recovery is once again faster in EVA40. The increase in dry days is less marked here, with a maximum change of about 3 days for EVA40$_{NH}$. Thus the resulting change in TP is mostly due to less intense rainfall.

The Maritime Continent is characterised by a fast and almost constant reduction in monthly precipitation (150-200 mm/month) and a slight increase in dry days in all EVA cases. Although this drying is less intense than over West Africa, the fact that it is persistent almost all year around and for at least 2 years could have severe consequences for water resources. Moreover, this risk is less sensitive to the eruption location, although the recovery seems faster in EVA40$_{SH}$.

Finally, for the Indian region, where monsoon precipitation is essential for agriculture and water resources, EVA40$_{NH}$, shows a 15-20% reduction in summer rainfall for at least 2 years along with a 50% increase in dry days. This signal is not observed in the other EVA cases, thus only Northern Hemisphere eruptions are expected to have a pronounced and sustained impact on drought persistence risk for India.

These changes around monsoonal area are consistent with what was previously found in [D'Agostino and Timmreck, 2022]. Here we could quantify more precisely how the ensemble is shifting from its normal state and how it persist over time in each region of interest.

4 Discussion

The above results are all based on simulations of a very large eruption (40 Tg of sulfur in the stratosphere). One might wonder if it is possible to linearly interpolate the results to lower (or higher) emission cases and thus estimate the risks for volcanic eruptions of different emission strengths. Results are displayed in Supplementary Fig. 6 for the two precipitation indices (TP and Rx5d) at regional scale for a tropical eruption, based on three additional simulation ensembles: EVA5, EVA10 and EVA20 with values linearly scaled to correspond to a 40Tg eruption (with numbers corresponding to the amount of sulfur injected into the stratosphere). The volcanic forcing has a similar spatial distribution in all cases just with a different overall strength.

Results show that although there is large uncertainties, the findings are consistent with a linear relationship. Risk ratios also show reasonable consistency, except for a few cases (for example TP over India). Thus, to first order, one can assume that results on extreme indices can likely be linearly interpolated if the volcanic forcing distribution is similar. However, when considering uncertainties represented by ensemble spreads, it is clear that lower emission cases (EVA5 and EVA10) are poorly detectable, even when scaled to EVA40. In these weaker cases the internal variability dominates the signals and the volcanic eruption fingerprint is less detectable. These simple results suggest it is not always possible to linearly scale results from EVA40 to other cases as the internal variability can become dominant and reduces the systemic impact of the volcanic eruption.

In this work we examined how very large, idealized eruptions could impact climate extremes in the three years following the eruption. Results are based on large ensembles from the MPI-ESM model, including simulations of three different volcano locations. In order to get a robust climate signal the idealized eruptions all have a common spatial pattern for the volcanic forcing for each location of eruption and in all simulations the eruptions occur in June, so any dependency on the particular pattern or seasonal timing, cannot be evaluated. While we expect these results to be representative of a typical tropical and NH (SH) extra tropical eruptions more simulations are therefore required to evaluate these potential limitations. The volcanic radiative effect is the only effect which we consider in our simulations by prescribing zonal and monthly mean optical parameters for every wavelength of the model's radiation scheme. Other indirect processes i.e interaction with atmospheric chemistry or potential cirrus modification (See for example [Robock, 2000, Timmreck et al., 2012, Kremser et al., 2016, Marshall et al., 2022]) are neglected, and the effect of these processes on extreme events could be further explored.

Our results are broadly consistent with other studies which have analysed large scale dynamical variability including Northern hemisphere winter warming [e.g. Coupe and Robock, 2021, Bittner et al., 2016, Azoulay et al., 2021], and a large effect on monsoon rainfall with a strong dependency on the hemisphere of the eruption[Zuo et al., 2019a, Haywood et al., 2013, Liu et al., 2016]. This study has benefited from the large number of simulations available to focus on the changing probability of extreme rare 1 in a century events, really highlighting the ability of large volcanic eruptions to cause events which would be unprecedented in recent history. While the model used here has been previously shown to have a good representation of forced and internal variability, it is very likely that another model could have given slightly different results, so given the importance of our findings,

repeating this study using a different model would be recommended. Volcanic induced changes can affect the tropical rain belt in a complex manner, via changes in surface conditions and in associated energy transport variations in the atmosphere and oceans (see for example [Erez and Adam, 2021]) and these simulations offer an excellent test bed for further analyses.

5 Conclusions

We have showed that, following a large eruption, the risk of centennial drought is greatly increased over several regions, especially West Africa, South and East Asia, and the Maritime Continent. These conditions are mainly due to a failure of monsoon precipitation (which can be half of normal expected rain) and can last for several years after the eruption. The risk of heavy rainfall tends to decrease over these regions, but by relatively smaller amounts. In other words, the large increase in drought risk is only slightly countered by a moderately reduced flooding risk.

Extreme Temperature results are consistent with previous studies [Robock and Mao, 1995, Paik and Min, 2017, Timmreck et al., 2012], with a reduced risk of hot extremes in summer. The risk of cold winter events was also found to be reduced in the Northern Hemisphere, corresponding to the winter warming signal observed previously [Robock and Mao, 1992].

Overall, changes in the risk of extremes is larger for a Northern Hemisphere eruption than for a tropical eruption, and a Southern Hemisphere eruption was found to have the weakest impact although there is also a regional dependency. Thus the location of the volcano is important to efficiently predict extreme events during the following years.

Finally, the ensemble response to the strength of a volcanic eruption cannot be linearly extrapolated to weaker eruption cases, as the internal variability of the atmosphere tends to become dominant. Thus, to estimate the change in risks it is important to simulate different eruption scenarios. Still, we noted that the ensemble mean response is close to linearity.

Our results indicate the severe impacts on agricultural systems in many areas of the world following a large eruption, and with several breadbasket regions affected (such as India and Eastern China) this could have a severe impact on food systems at a global scale. We therefore strongly recommend that other modelling groups conduct similar idealized experiments so that a broader assessment of the robustness of the results can be evaluated.

Acknowledgements

Discussions with Roberta d'Agostino, Gabi Hegerl and Dirk Olonscheck are gratefully acknowledged. Claudia Timmreck is supported by the DFG research unit FOR 2820: Revisiting The Volcanic Impact on Atmosphere and Climate – Preparations for the Next Big Volcanic Eruption (VolImpact, project number:398006378). MPI-ESM computations were performed on the computer of the Deutsches Klima Rechenzentrum (DKRZ) using resources granted by its Scientific Steering Committee (WLA) under project ID bb1093. A S and A B were funded by the NERC project GloSAT (NE/S015698/1) and A S and N F received funding from a Chancellors fellowship at the University of Edinburgh. We thank the two anonymous reviewers for their helpful comments.

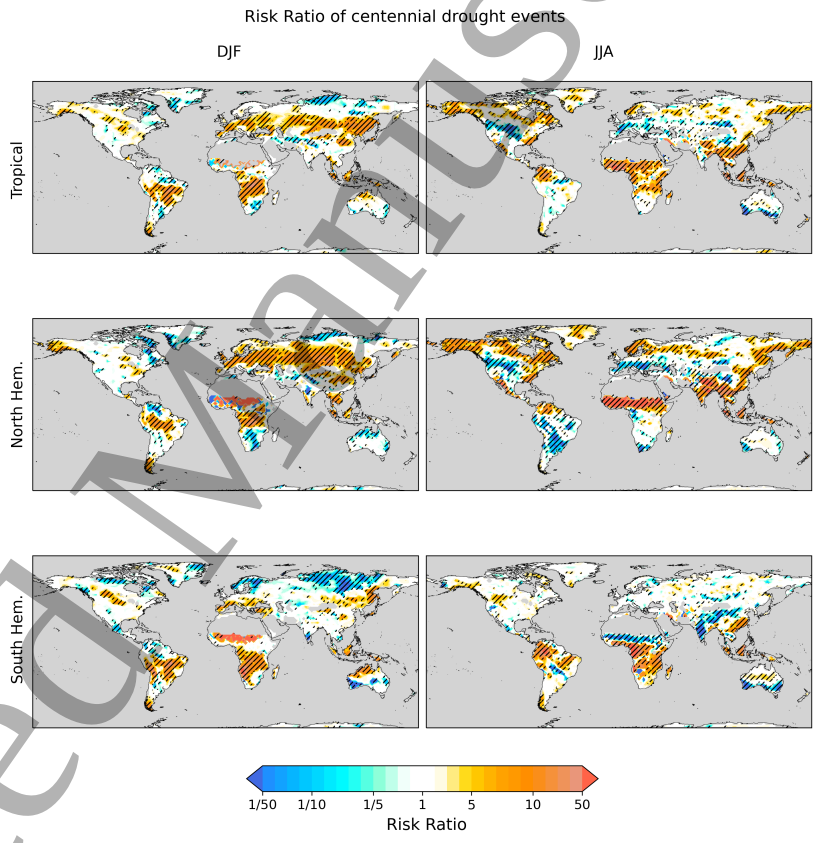

Figure 1: Risk ratio (EVA40 over EVA0) of centennial minimum accumulated monthly precipitation. Diagonal hatching indicate results at 95% confidence level. Sea and desert areas (where precipitation is below 250mm/year) are masked.

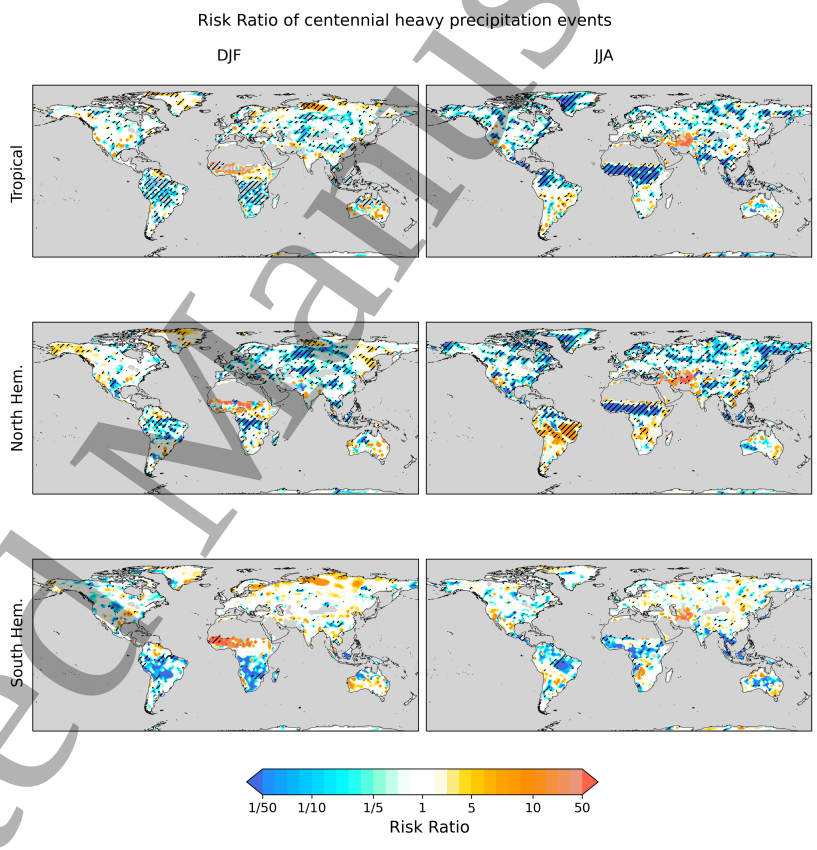

Figure 2: Same as Fig. 1 but for centennial 5-day maximum accumulated precipitation.

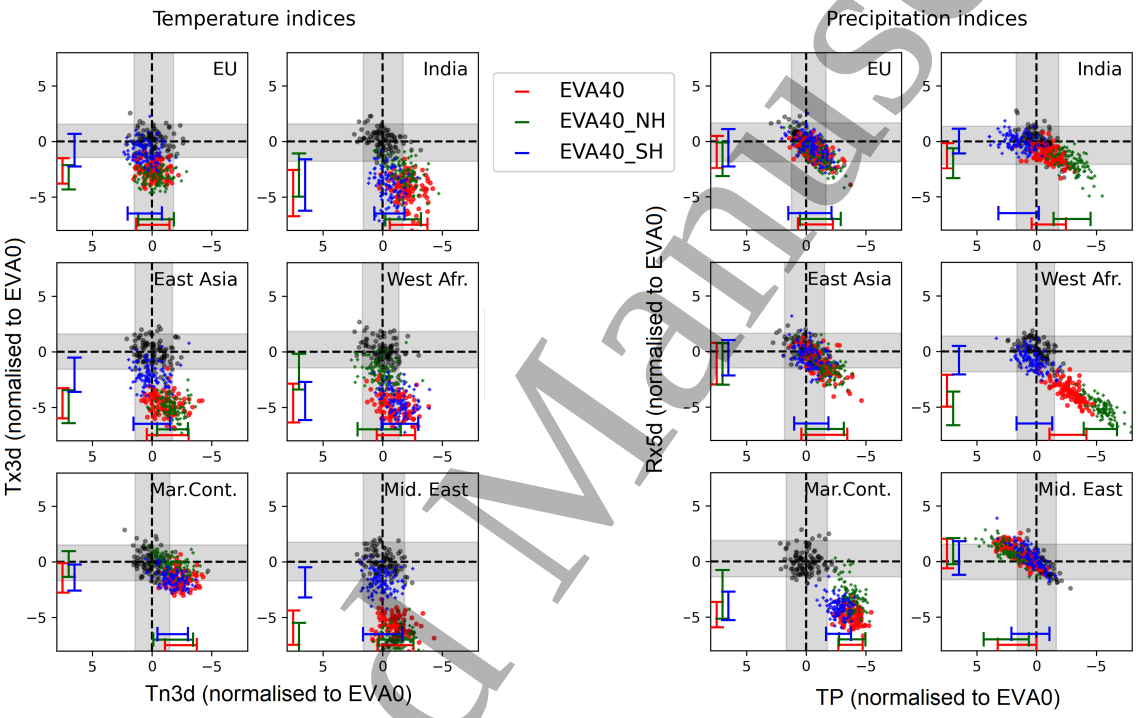

Figure 3: Scatter plot showing changes in different indices at regional scale. Indices are selected for the whole year following the eruption (Jan+1 - Dec+1). Each coloured symbol corresponds to a single model ensemble member, with colours corresponding to different EVA cases (black, red, green and blue, for EVA0, EVA40, EVA40$_{NH}$ and EVA40$_{SH}$ respectively). All results are displayed as anomalies relative to EVA0 and normalised by EVA0 standard deviation. Gray shading indicates the 5-95 percentile interval of EVA0 ensemble while lateral coloured bars indicate the 5-95 percentile interval for each EVA40 ensemble. Note that the direction of the axes have been reversed for Tn3d and TP, so values to the right reflect increased cold surges and drought, respectively.

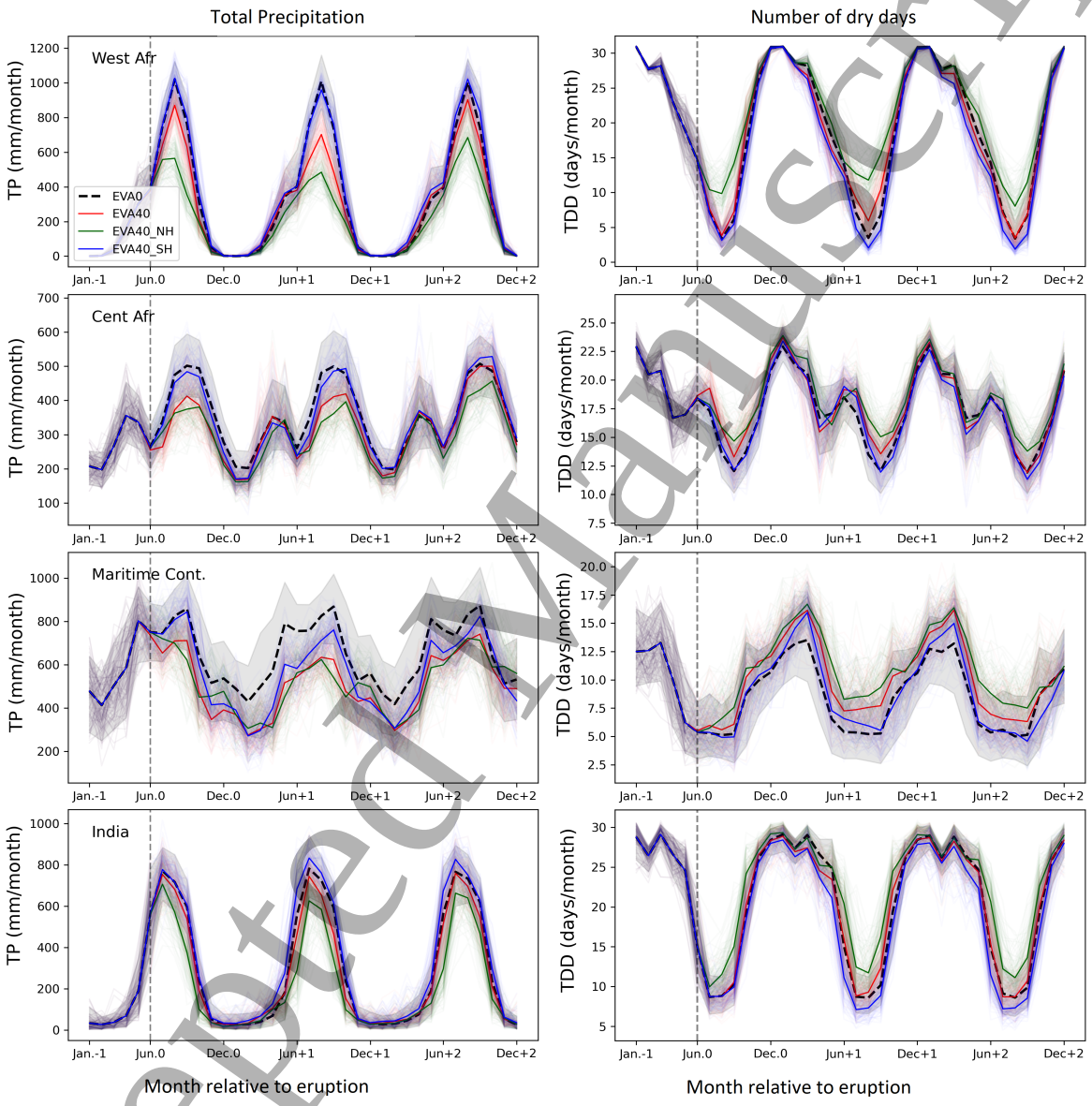

Figure 4: Time series of monthly TP (left) and TDD (right) averaged over different regions. Thick and thin lines show the ensemble means and individual members respectively. Gray shading indicates the 5-95 percentile interval of EVA0 ensemble.

Table 1: Indices used in this study. For each index, the statistic computed over a given period of time is specified. For example, "maximum" indicates the maximum value of the index during a season (or a year etc...) is selected. The last column provides a short description of the index.

Index name	**Definition**	**Statistic analyzed**	**Description**
Rx5d (mm/5-day)	5-day precipitation	Maximum	Persistent heavy precipitation (flood risks)
TP (mm/month)	Total precipitation	Mean	Accumulated precipitation (droughts)
TDD (number of days)	Total dry days (<1 mm)	Sum	Accumulation of water deficit (drought risks)
Tn3d (°C)	3-day mean temperature	Minimum	Persistent cold (cold surges)
Tx3d (°C)	3-day mean temperature	Maximum	Persistent heat (heat waves)

References

A. Azoulay, H. Schmidt, and C. Timmreck. The arctic polar vortex response to volcanic forcing of different strengths. *Journal of Geophysical Research: Atmospheres*, 126(11):e2020JD034450, 2021.

M. Bittner, H. Schmidt, C. Timmreck, and F. Sienz. Using a large ensemble of simulations to assess the northern hemisphere stratospheric dynamical response to tropical volcanic eruptions and its uncertainty. *Geophysical Research Letters*, 43(17):9324–9332, 2016.

S. Brönnimann, J. Franke, S. U. Nussbaumer, H. J. Zumbühl, D. Steiner, M. Trachsel, G. C. Hegerl, A. Schurer, M. Worni, A. Malik, et al. Last phase of the little ice age forced by volcanic eruptions. *Nature geosciences*, 12(8):650–656, 2019.

S. Brönnimann, P. Stucki, J. Franke, V. Valler, Y. Brugnara, R. Hand, L. C. Slivinski, G. P. Compo, P. D. Sardeshmukh, M. Lang, et al. Influence of warming and atmospheric circulation changes on multidecadal european flood variability. *Climate of the Past*, 18(4):919–933, 2022.

J. Coupe and A. Robock. The influence of stratospheric soot and sulfate aerosols on the northern hemisphere wintertime atmospheric circulation. *Journal of Geophysical Research: Atmospheres*, 126 (11):e2020JD034513, 2021. doi: https://doi.org/10.1029/2020JD034513.

R. D'Agostino and C. Timmreck. Sensitivity of regional monsoons to idealised equatorial volcanic eruption of different sulfur emission strengths. *ERL*, page 17: 054001, 2022. doi: 10.1088/1748-9326/ac62af.

C. Deser, F. Lehner, K. B. Rodgers, T. Ault, T. L. Delworth, P. N. DiNezio, A. Fiore, C. Frankignoul, J. C. Fyfe, D. E. Horton, et al. Insights from earth system model initial-condition large ensembles and future prospects. *Nature Climate Change*, 10(4):277–286, 2020.

M. Erez and O. Adam. Energetic constraints on the time-dependent response of the itcz to volcanic eruptions. *Journal of Climate*, pages 9989–10006, 2021. doi: https://doi.org/10.1175/JCLI-D-21-0146.1.

S. Fadnavis, R. Müller, T. Chakraborty, T. P. Sabin, A. Laakso, A. Rap, S. Griessbach, J.-P. Vernier, and S. Tilmes. The role of tropical volcanic eruptions in exacerbating indian droughts. *Scientific reports*, 11(2714), 2021.

E. M. Fischer, S. Sippel, and R. Knutti. Increasing probability of record-shattering climate extremes. *Nature Climate Change*, 11:689–695, 2021.

F. Gaupp, J. Hall, D. Mitchell, and S. Dadson. Increasing risks of multiple breadbasket failure under 1.5 and 2°c global warming. *Agricultural Systems*, 175:34–45, 2019.

J. M. Haywood, A. Jones, N. Bellouin, and S. D. Asymmetric forcing from stratospheric aerosols impacts sahelian rainfall. *Nat. Clim. Change*, 3(7):660–665, 2013. doi: https://doi:10.1038/nclimate1857.

C. E. Iles and G. C. Hegerl. The global precipitation response to volcanic eruptions in the cmip5 models. *Environmental Research Letters*, 9(10):104012, 2014.

C. E. Iles and G. C. Hegerl. Systematic change in global patterns of streamflow following volcanic eruptions. *Nature Geoscience*, 8(11):838–842, 2015.

M. Iturbide, J. M. Gutiérrez, L. M. Alves, J. Bedia, R. Cerezo-Mota, E. Cimadevilla, A. S. Cofiño, A. Di Luca, S. H. Faria, I. V. Gorodetskaya, M. Hauser, S. Herrera, K. Hennessy, H. T. Hewitt, R. G. Jones, S. Krakovska, R. Manzanas, D. Martínez-Castro, G. T. Narisma, I. S. Nurhati, I. Pinto, S. I. Seneviratne, B. van den Hurk, and C. S. Vera. An update of ipcc climate reference regions for subcontinental analysis of climate model data: definition and aggregated datasets. *Earth System Science Data*, 12(4):2959–2970, 2020. doi: 10.5194/essd-12-2959-2020. URL `https://essd.copernicus.org/articles/12/2959/2020/`.

T. W. P. Jacobson, W. Yang, G. A. Vecchi, and L. W. Horowitz. Impact of volcanic aerosol hemispheric symmetry on sahel rainfall. *Climate Dynamics*, 55:1733–1758, 2020.

R. Joseph and N. Zeng. Seasonally modulated tropical drought induced by volcanic aerosol. *Journal of Climate*, 24(8):2045–2060, 2011.

J. H. Jungclaus, N. Fischer, H. Haak, K. Lohmann, J. Marotzke, D. Matei, U. Mikolajewicz, D. Notz, and J. Von Storch. Characteristics of the ocean simulations in the max planck institute ocean model

(mpiom) the ocean component of the mpi-earth system model. *Journal of Advances in Modeling Earth Systems*, 5(2):422–446, 2013.

S. Kremser, L. W. Thomason, M. von Hobe, M. Hermann, T. Deshler, C. Timmreck, M. Toohey, A. Stenke, J. P. Schwarz, R. Weigel, S. Fueglistaler, F. J. Prata, J.-P. Vernier, H. Schlager, J. E. Barnes, J.-C. Antuña-Marrero, D. Fairlie, M. Palm, E. Mahieu, J. Notholt, M. Rex, C. Bingen, F. Vanhellemont, A. Bourassa, J. M. C. Plane, D. Klocke, S. A. Carn, L. Clarisse, T. Trickl, R. Neely, A. D. James, L. Rieger, J. C. Wilson, and B. Meland. Stratospheric aerosol—observations, processes, and impact on climate. *Reviews of Geophysics*, 54(2):278–335, 2016. doi: https://doi.org/10.1002/2015RG000511.

C. A. Kroll, S. Dacie, A. Azoulay, H. Schmidt, and C. Timmreck. The impact of volcanic eruptions of different magnitude on stratospheric water vapor in the tropics. *Atmospheric Chemistry and Physics*, 21(8):6565–6591, 2021.

F. Liu, J. Chai, B. Wang, J. Liu, X. Zhang, and W. Z. Global monsoon precipitation responses to large volcanic eruptions. *Scientific reports*, 6(17):24331, 2016. doi: doi:10.1038/srep24331.

N. Maher, S. Milinski, L. Suarez-Gutierrez, M. Botzet, M. Dobrynin, L. Kornblueh, J. Kröger, Y. Takano, R. Ghosh, C. Hedemann, et al. The max planck institute grand ensemble: enabling the exploration of climate system variability. *Journal of Advances in Modeling Earth Systems*, 11(7): 2050–2069, 2019.

W. Man, T. Zhou, and J. H. Jungclaus. Effects of large volcanic eruptions on global summer climate and east asian monsoon changes during the last millennium: Analysis of mpi-esm simulations. *Journal of Climate*, 27(19):7394–7409, 2014.

L. R. Marshall, E. C. Maters, and C. R. A. T. M. Schmidt, A.and Timmreck. Volcanic effects on climate: recent advances and future avenues. *Bulletin of Volcanology*, 84(54), 2022. doi: doi.org/10.1007/s00445-022-01559-3.

S. Milinski, N. Maher, and D. Olonscheck. How large does a large ensemble need to be? *Earth System Dynamics*, 11(4):885–901, 2020.

N. A. of Sciences, Engineering, and Medicine. *Attribution of Extreme Weather Events in the Context of Climate Change*. The National Academies Press, Washington, DC, 2016. ISBN 978-0-309-38094-2.

F. Otto, S. Philip, S. Kew, L. S., K. A., and C. H. Attributing high-impact extreme events across timescales—a case study of four different types of events. *Climatic Change*, 149:399–412, 2018. doi: https://doi.org/10.1007/s10584-018-2258-3.

S. Paik and S.-K. Min. Climate responses to volcanic eruptions assessed from observations and cmip5 multi-models. *Climate Dynamics*, 48(3):1017–1030, 2017.

S. Paik and S.-K. Min. Assessing the impact of volcanic eruptions on climate extremes using cmip5 models. *Journal of Climate*, 31(14):5333–5349, 2018.

S. Paik, S.-K. Min, C. E. Iles, E. M. Fischer, and A. P. Schurer. Volcanic-induced global monsoon drying modulated by diverse el niño responses. *Science advances*, 6(21):eaba1212, 2020.

I. Quaglia, C. Timmreck, U. Niemeier, D. Visioni, G. Pitari, C. Brodowsky, C. Brühl, S. S. Dhomse, H. Franke, A. Laakso, et al. Interactive stratospheric aerosol models' response to different amounts and altitudes of so 2 injection during the 1991 pinatubo eruption. *Atmospheric Chemistry and Physics*, 23(2):921–948, 2023.

C. Raymond, J. Horton, Radley M.and Zscheischler, O. Martius, A. AghaKouchak, J. Balch, S. G. Bowen, S. J. Camargo, J. Hess, K. Kornhuber, M. Oppenheimer, A. C. Ruane, T. Wahl, and K. White. Understanding and managing connected extreme events. *Nature Climate Change*, 10(7): 1758–6798, 2020.

C. Raymond, L. Suarez-Gutierrez, K. Kornhuber, M. Pascolini-Campbell, J. Sillmann, and D. E. Waliser. Increasing spatiotemporal proximity of heat and precipitation extremes in a warming world quantified by a large model ensemble. *Environmental Research Letters*, 17(3):035005, 2022.

C. Reick, T. Raddatz, V. Brovkin, and V. Gayler. Representation of natural and anthropogenic land cover change in mpi-esm. *Journal of Advances in Modeling Earth Systems*, 5(3):459–482, 2013.

A. Robock. Volcanic eruptions and climate. *Reviews of geophysics*, 38(2):191–219, 2000.

A. Robock and J. Mao. Winter warming from large volcanic eruptions. *Geophysical Research Letters*, 19(24):2405–2408, 1992.

A. Robock and J. Mao. The volcanic signal in surface temperature observations. *Journal of Climate*, 8(5):1086–1103, 1995.

M. Sigl, M. Toohey, J. R. McConnell, J. Cole-Dai, and M. Severi. Volcanic stratospheric sulfur injections and aerosol optical depth during the holocene (past 11,500 years) from a bipolar ice core array. *Earth System Science Data Discussions*, pages 1–45, 2022.

B. Stevens, M. Giorgetta, M. Esch, T. Mauritsen, T. Crueger, S. Rast, M. Salzmann, H. Schmidt, J. Bader, K. Block, et al. Atmospheric component of the mpi-m earth system model: Echam6. *Journal of Advances in Modeling Earth Systems*, 5(2):146–172, 2013.

L. Suarez-Gutierrez, W. A. Müller, C. Li, and J. Marotzke. Hotspots of extreme heat under global warming. *Climate Dynamics*, 55:429–447, 2020.

L. Suarez-Gutierrez, S. Milinski, and N. Mayer. Exploiting large ensembles for a better yet simpler climate model evaluation. *Climate Dynamics*, 57:2557–2580, 2021.

K. E. Taylor, R. J. Stouffer, and G. A. Meehl. An overview of cmip5 and the experiment design. *Bulletin of the American meteorological Society*, 93(4):485–498, 2012.

C. Timmreck, H.-F. Graf, D. Zanchettin, S. Hagemann, T. Kleinen, and K. Krüger. Climate response to the toba super-eruption: Regional changes. *Quaternary International*, 258:30–44, 2012.

M. Toohey and M. Sigl. Volcanic stratospheric sulfur injections and aerosol optical depth from 500 bce to 1900 ce. *Earth System Science Data*, 9(2):809–831, 2017.

M. Toohey, K. Krüger, M. Bittner, C. Timmreck, and H. Schmidt. The impact of volcanic aerosol on the northern hemisphere stratospheric polar vortex: mechanisms and sensitivity to forcing structure. *Atmospheric Chemistry and Physics*, 14(23):13063–13079, 2014.

K. E. Trenberth and A. Dai. Effects of mount pinatubo volcanic eruption on the hydrological cycle as an analog of geoengineering. *Geophysical Research Letters*, 34(15), 2007.

T. Wang, J. Miao, H. Wang, and J. Sun. Influence of strong tropical volcanic eruptions on daily temperature and precipitation extremes across the globe. *Journal of Meteorological Research*, 35: 428–443, 2021.

P. R. Wood, F. Lehner, A. G. Pendergrass, and S. Schlunegger. Changes in precipitation variability across time scales in multiple global climate model large ensembles. *Environmental Research Letters*, 16(8):084022, 2021.

Z. Zhuo, I. Kirchner, S. Pfahl, and U. Cubasch. Climate impact of volcanic eruptions: the sensitivity to eruption season and latitude in mpi-esm ensemble experiments. *Atmospheric Chemistry and Physics*, 21(17):13425–13442, 2021.

M. Zuo, T. Zhou, and W. Man. Hydroclimate responses over global monsoon regions following volcanic eruptions at different latitudes. *Journal of Climate*, 32(14):4367—-4385, 2019a.

M. Zuo, T. Zhou, and W. Man. Wetter global arid regions driven by volcanic eruptions. *JGR Atmospheres*, 124(24):13648–13662, 2019b.

F. W. Zwiers and V. V. Kharin. Changes in the extremes of the climate simulated by ccc gcm2 under co2 doubling. *Journal of Climate*, 11(9):2200–2222, 1998.